Magnetic domain wall skyrmions

Ran Cheng,[1,2] Maxwell Li,[3] Arjun Sapkota,[4] Anish Rai,[4] Ashok Pokhrel,[4] Tim Mewes,[4] Claudia Mewes,[4] Di Xiao,[1,3] Marc De Graef,[3] and Vincent Sokalski[3]

[1]*Department of Physics, Carnegie Mellon University, Pittsburgh, Pennsylvania 15213, USA*
[2]*Department of Electrical & Computer Engineering, University of California, Riverside, California 92521, USA*
[3]*Department of Materials Science & Engineering, Carnegie Mellon University, Pittsburgh, Pennsylvania 15213, USA*
[4]*Department of Physics and Astronomy/MINT Center, The University of Alabama, Tuscaloosa, Alabama 35487, USA*

(Received 10 September 2018; published 13 May 2019)

It is well established that the spin-orbit interaction in heavy metal/ferromagnet heterostructures leads to a significant interfacial Dzyaloshinskii-Moriya interaction (DMI), which modifies the internal structure of magnetic domain walls (DWs) to favor Néel- over Bloch-type configurations. However, the impact of such a transition on the structure and stability of internal DW defects (e.g., vertical Bloch lines) needs to be explored. We present a combination of analytical and micromagnetic calculations to describe a type of topological excitation called a DW skyrmion characterized by a 360° rotation of the internal magnetization in a Dzyaloshinskii DW. We further propose a method to identify DW skyrmions experimentally using Fresnel-mode Lorentz transmission electron microscopy; simulated images of DW skyrmions using this technique are presented based on the micromagnetic results.

DOI: 10.1103/PhysRevB.99.184412

I. INTRODUCTION

The discovery of a large Dzyaloshinskii-Moriya interaction (DMI) [1,2] in bulk magnetic crystals [3,4] and thin films with structural inversion asymmetry [5–8] has led to a fervent rebirth of research on magnetic bubble domains in the form of smaller particlelike features called skyrmions, which are minimally defined as having an integer-valued topological charge Q, computed from $4\pi\, Q = \int dxdy\, \mathbf{m} \cdot (\partial_x \mathbf{m} \times \partial_y \mathbf{m})$, where $\mathbf{m}$ is the unit magnetization vector. Although nontrivial to calculate, there is an inherent energy barrier associated with the annihilation of such an object when Q goes to 0—something widely referred to as topological protection. The combination of a large DMI, which yields smaller, more stable skyrmions, and a related spin-orbit coupling phenomenon, viz., the spin Hall effect [9–12], makes the prospect of using skyrmions for energy-efficient memory and computing attractive [13,14].

Here, we present a manifestly different type of topologically protected magnetic excitation called a domain wall (DW) skyrmion, which has previously been considered under a field-theory context [15,16]. It describes a 360° wind of the DW's internal magnetization along the wall profile and has a topological charge of ± 1. In the absence of DMI, DWs in thin films with perpendicular magnetic anisotropy tend to form the Bloch configuration [17]. In these walls, it is common to encounter topological defects ($Q = \pm\frac{1}{2}$) characterized by 180° transitions called vertical Bloch lines (VBLs), as shown in Figs. 1(a) and 1(b) [18,19], which were once considered in their own right for computer memory [20,21]. Adding a sufficiently strong interfacial DMI, however, will favor a Néel-type DW with preferred chirality, known as the Dzyaloshinskii DW [5]. Correspondingly, a VBL in the presence of DMI will become a DW skyrmion as schematically illustrated in Figs. 1(c) and 1(d). In contrast to conventional skyrmions that can propagate along any direction in two dimensions (2D) and are subject to the skyrmion Hall effect [22], a DW skyrmion can only move in reconfigurable 1D channels defined by the network of magnetic DWs. Moreover, the interfacial DMI substantially reduces the exchange length along the DW, resulting in a DW skyrmion that is much smaller than its VBL predecessor—an observation analogous to 2D skyrmions and magnetic bubbles. It is worth noting that unlike the conventional 2D skyrmions that can form a lattice as the ground state [23], DW skyrmions can only be metastable excitations. Their existence in systems with a strong DMI needs to be investigated.

This paper describes the static properties of DW skyrmions and proposes a methodology to identify them experimentally. We begin with an analytical solution of the DW skyrmion profile obtained by energy minimization, which is found to match well with micromagnetic solutions. Based on the micromagnetic output, Lorentz transmission electron microscopy (LTEM) images are simulated showing that DW skyrmions should present a clear signature in the Fresnel observation mode.

II. ANALYTICAL CALCULATIONS

We choose Cartesian coordinates such that the DW normal is along x and the film normal is z (Fig. 1). In the thin-film approximation, by assuming that the system is uniform in the thickness direction and infinite along y, we have the free energy in the continuum limit as

$$\frac{E}{t_F} = \int dxdy \Big\{ A \sum_i |\partial_i \boldsymbol{m}|^2 + D\boldsymbol{m} \cdot [(\hat{z} \times \boldsymbol{\nabla}) \times \boldsymbol{m}] - K m_z^2 + \frac{\ln 2}{2\pi} \frac{t_F}{\lambda} \mu_0 M_s^2 [\hat{\boldsymbol{n}}(y) \cdot \boldsymbol{m}]^2 \Big\}, \quad (1)$$

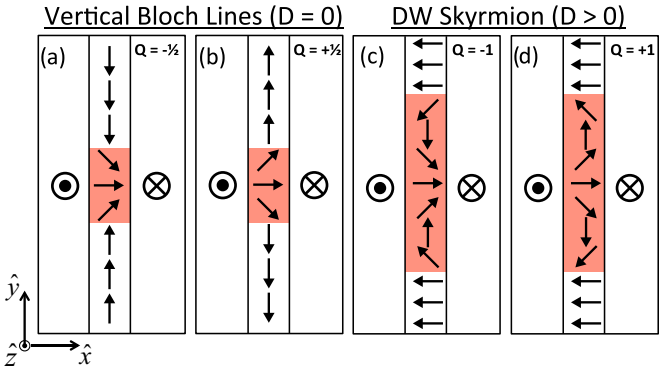

FIG. 1. Comparison of (a), (b) vertical Bloch lines and (c), (d) DW skyrmions, which result from interfacial DMI.

where t_F is the film thickness, A is the exchange stiffness, $i = x, y, z$, D is the DMI, M_s is the saturation magnetization, and $K = K_u - \mu_0 M_s^2/2$ is the effective perpendicular magnetic anisotropy with K_u the intrinsic magnetocrystalline anisotropy. The last term represents the demagnetization energy approximated in the thin-film geometry [5,19,24], where $\lambda = \sqrt{A/K}$ is the exchange length [25] and $\hat{\boldsymbol{n}}(y)$ is a *local* normal vector of the DW to account for distortion [26] in the presence of an internal topological defect.

To solve for $\boldsymbol{m} = \boldsymbol{m}(x, y)$, we parametrize the magnetization vector in spherical coordinates as

$$\boldsymbol{m} = \{\sin\theta\cos\phi, \sin\theta\sin\phi, \cos\theta\}. \tag{2}$$

In the absence of DMI ($D = 0$), minimizing the free energy leads to a standard soliton profile, $\theta = 2\arctan\exp(x/\lambda)$ and $\phi = \pm\pi/2$, with $\pm$ representing a Bloch wall of either chirality.

Adding a strong DMI will overcome the demagnetization energy, leading to Néel walls with either $\phi = 0$ or π. Here, we choose $D > 0$, thus $\phi = \pi$ at $y = \pm\infty$. As ϕ changes, VBLs [Figs. 1(a) and 1(b)] will gradually transition into DW skyrmions [Figs. 1(c) and 1(d)]. Similar to constriction of the DW profile in a VBL due to the increased demagnetization energy [26], the presence of a DW skyrmion also locally deforms the DW profile due to DMI. Because the internal magnetization is inevitably tilted away from the DW normal in a DW skyrmion, there is a driving force for the DW itself to bend locally as an attempt to recover this energy; this phenomenon is similar to the spontaneous tilting of Dzyaloshinskii DWs identified in Refs. [7,27]. To capture this effect, we adopt a modified Slonczewski ansatz for the profile function that involves two independent variables,

$$\theta = 2\arctan\exp\frac{x - q(y)}{\lambda}, \tag{3}$$

$$\phi = \phi(y), \tag{4}$$

where $\phi(y)$ is the azimuthal angle of the in-plane component of $\boldsymbol{m}$ and $q(y)$ denotes the deviation of the DW center from its location in a straight homochiral DW without a VBL or DW skyrmion; $q(y)$ and $\phi(y)$ are two collective coordinates to be solved by minimizing the total energy. We have neglected a possible y dependence of λ, which is expected to become significant only for large DMI. Inserting Eqs. (3) and (4) into the energy functional Eq. (1), noting that the local normal vector $\hat{\boldsymbol{n}} = \{1, q', 0\}/\sqrt{1 + q'^2}$, and integrating out x from $-\infty$ to ∞, we obtain the free energy

$$E = \frac{2t_F A}{\lambda}\int dy[q'^2 + \lambda^2\phi'^2 + 2\xi(\cos\phi - q'\sin\phi) + 2\eta(\cos^2\phi - q'\sin 2\phi)], \tag{5}$$

where $\xi = \pi D/4\sqrt{AK}$ and $\eta = (\ln 2)t_F\mu_0 M_s^2/4\pi\sqrt{AK}$ are two dimensionless parameters characterizing the strengths of the DMI and the demagnetization energy relative to the DW energy $4\sqrt{AK}$. In typical ferromagnets, ξ and η are small so we only keep linear order terms for these parameters in Eq. (5).

Minimizing the free energy calls for two Euler-Lagrange equations. The first one, $\delta_q E = 0$, yields $q' - \xi\sin\phi - \eta\sin 2\phi = C$, where the constant C can be determined by the boundary conditions. At $y \to \pm\infty$, we have $q' \to 0$ and $\phi \to -\arccos(\xi/2\eta)$, thus $C = 0$. Including the other equation, $\delta_\phi E = 0$, we arrive at two coupled nonlinear differential equations,

$$-\lambda^2\phi'' = \xi(\sin\phi + q'\cos\phi) + \eta(\sin 2\phi + 2q'\cos 2\phi), \tag{6}$$

$$q' = \xi\sin\phi + \eta\sin 2\phi. \tag{7}$$

Since Eq. (5) is accurate to linear order in ξ and η, we ignore quadratic terms of ξ and η in Eqs. (7) and (6), by which ϕ effectively decouples from q. Then Eq. (7) reduces to a double sine-Gordon equation that, despite high nonlinearity, can be solved analytically. Defining $\beta = \xi/2\eta$ as the relative strength of DMI with respect to the demagnetization energy, we obtain our central results:

$$\frac{\phi}{2} = \begin{cases} \pm\arctan\left[\sqrt{\frac{1+\beta}{1-\beta}}\tanh\left(\frac{1}{2}\sqrt{1-\beta^2}y/\lambda_s\right)\right] & \text{if } \beta < 1, \\ \pm\arctan\left[\sqrt{\frac{\beta}{\beta-1}}\sinh\left(\sqrt{\beta-1}y/\lambda_s\right)\right] & \text{if } \beta \geqslant 1, \end{cases} \tag{8}$$

and

$$\frac{q}{\lambda_s} = \begin{cases} 2\eta(1+\beta)\frac{\cosh(\sqrt{1-\beta^2}y/\lambda_s)-1}{\cosh(\sqrt{1-\beta^2}y/\lambda_s)-\beta} & \text{if } \beta < 1, \\ 4\eta\sqrt{\beta}\left[1 + \frac{(\beta-1)\cosh\left(\sqrt{\beta-1}y/\lambda_s\right)}{1-\beta\cosh^2\left(\sqrt{\beta-1}y/\lambda_s\right)}\right] & \text{if } \beta \geqslant 1, \end{cases} \tag{9}$$

where $\lambda_s = \lambda/\sqrt{2\eta}$ is an exchange length along y at the critical point $\beta = 1$ and the $+(-)$ sign represents the solution with positive (negative) topological charge Q. The critical condition $\beta = 1$ is where the Néel wall is formed at $y \to \pm\infty$ and a DW skyrmion with $Q = \pm 1$ is formed at the center. At this value, $\phi/2 \to \pm\arctan y/\lambda_s$ and $q/\lambda_s \to \frac{4\eta(y/\lambda_s)^2}{1+(y/\lambda_s)^2}$. For $\beta < 1$, only a partial DW skyrmion with $1/2 \leqslant |Q| < 1$ exists and $\phi(\pm\infty) = \pm[\pi - \arccos(\beta)]$. For $\beta = 0$, Eqs. (8) and (9) reduce to a VBL profile [18,19]. When converted into original units, the critical condition becomes

$$D_c = \frac{2\ln 2}{\pi^2}t_F\mu_0 M_s^2, \tag{10}$$

which sets a minimum DMI strength to form a full DW skyrmion. To characterize the impact of DMI on the DW skyrmion energy ΔE (i.e., the energy cost of creating a

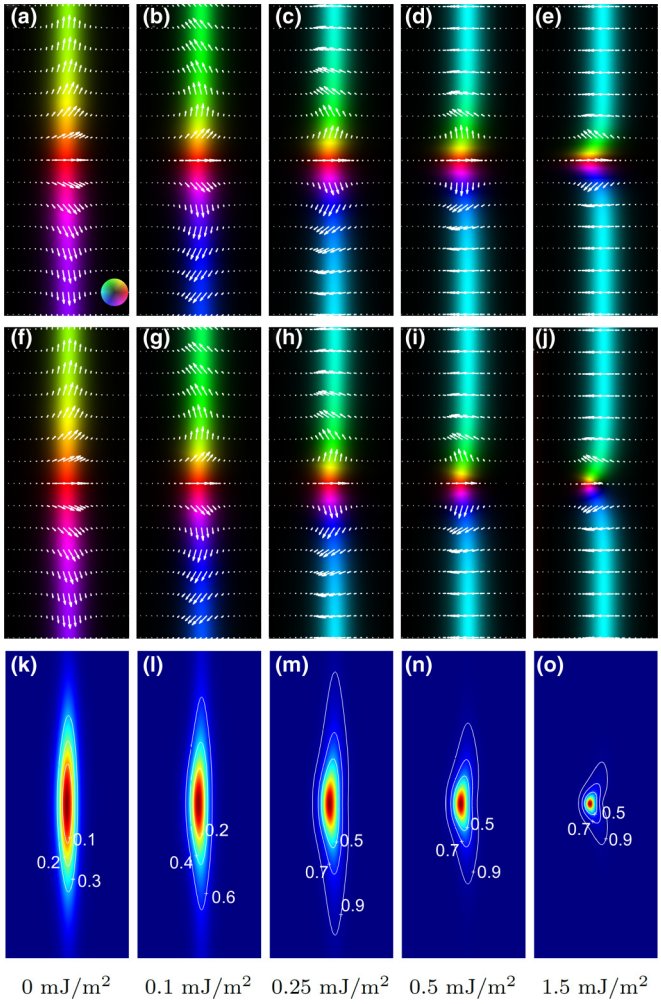

FIG. 2. (a)–(e) Analytical solutions Eqs. (8) and (9). (f)–(j) Full micromagnetic solutions. Arrows indicate the in-plane component of the magnetization. (k)–(o) Normalized topological charge densities: Here, the contour lines enclose the topological charge indicated. The DMI strength is indicated at the bottom of each column. The areas shown are 100 nm × 250 nm.

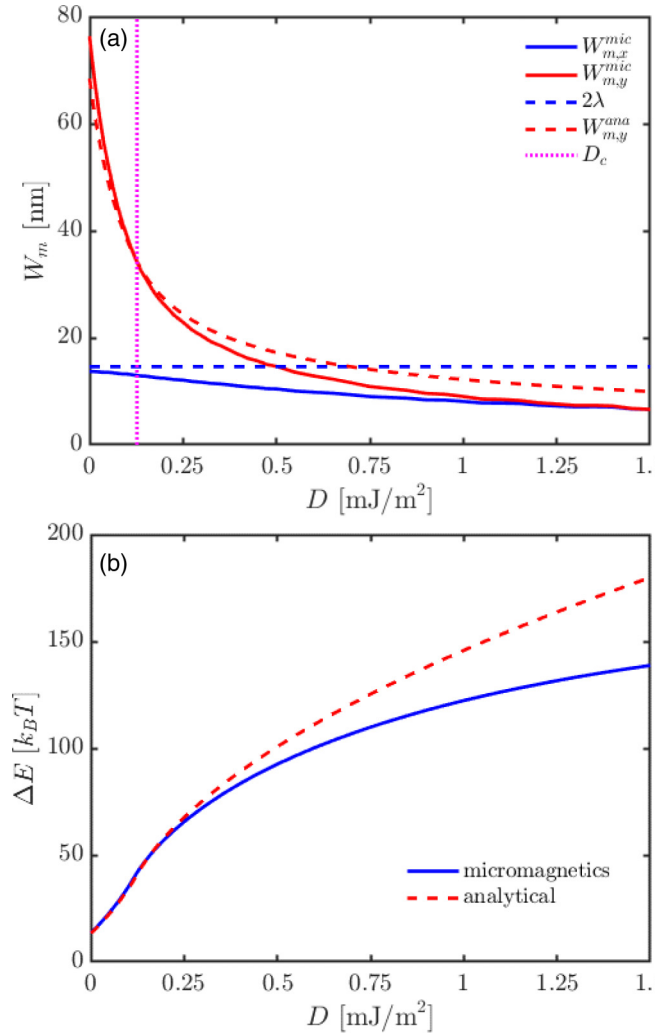

FIG. 3. (a) DW skyrmion width $W_{m,x}$ (blue) across and $W_{m,y}$ (red) along the domain wall as a function of DMI strength for micromagnetic (solid lines) and analytical (dashed lines) calculations. The critical DMI strength D_c is shown as a dotted magenta line. (b) Corresponding DW skyrmion energy vs DMI. Parameters used were $t_F = 2$ nm, $K = 3 \times 10^5$ J/m^3, $A = 1.6 \times 10^{-11}$ J/m, and $M_s = 600$ kA/m.

DW skyrmion inside a DW), we normalize by the VBL energy ΔE_{VBL}. [17–19] This leads to a rather simple form of the scaled DW skyrmion energy,

$$\frac{\Delta E}{\Delta E_{\mathrm{VBL}}} = \begin{cases} \sqrt{1-\beta^2} + 2\beta \arctan\sqrt{\frac{1+\beta}{1-\beta}} & \text{if } \beta < 1, \\ 2\sqrt{\beta-1} + 2\beta \operatorname{arccsc}\sqrt{\beta} & \text{if } \beta \geqslant 1, \end{cases} \tag{11}$$

which is plotted in Fig. 3(b) along with the corresponding micromagnetic calculations to be discussed below.

III. MICROMAGNETIC CALCULATIONS

We used our MATLAB-based finite-differences code M^3 [28,29]. The code implements the Dzyaloshinskii-Moriya interaction for thin films and the corresponding boundary conditions [30], together with the exchange interaction for micromagnetics [31]. As can be seen in Fig. 2, the magnetization profile of the analytic solutions agrees well with the full micromagnetic results, including the notchlike deformation near the center which ascribes to an increasing D. The parameters used in these calculations are as follows: $t_F = 2$ nm, $K = 3 \times 10^5$ J/m^3, $A = 1.6 \times 10^{-11}$ J/m, and $M_s = 600$ kA/m, which are comparable to values reported for Co/Ni multilayers in Refs. [7,8]. The total volume simulated was 128 nm × 512 nm × 2 nm and the cell size was 0.5 nm × 0.5 nm × 2 nm. In regard to future applications, the size of a skyrmion plays an important role. A conventional skyrmion, i.e., a Néel- or Bloch-type skyrmion, consists of an inner and outer domain as well as a DW separating them. The skyrmion size is often given by its radius which is defined by the inner area bounded by the contour for which the out-of-plane magnetization vanishes, thereby neglecting the wall width [32]. Because the DW skyrmion is confined within a distorted DW (Fig. 2), the conventional definition of a single skyrmion radius is not applicable. However, one can use the

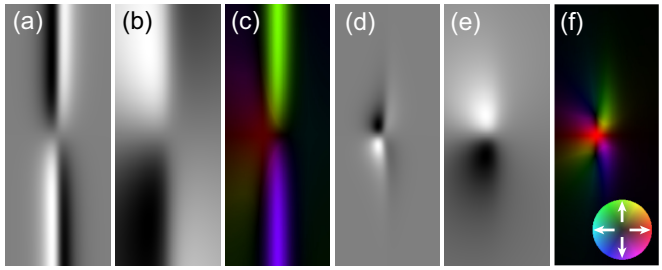

FIG. 4. (a) and (d) Fresnel-mode LTEM, (b) and (e) phase map, and (c) and (f) in-plane magnetic induction map of (a)–(c) a vertical Bloch line ($D = 0$ mJ/m^2) and (d)–(f) DW skyrmion ($D = 0.5$ mJ/m^2) calculated from the micromagnetic output of Figs. 2(f) and 2(i).

DW width $W_{m,x}$ at the skyrmion center and the width of the DW substructure $W_{m,y}$ along the wall to obtain an estimate of the size of the DW skyrmion (for details, see the Supplemental Material [33]). As shown in Fig. 3, both quantities decrease with increasing DMI. For the analytical solution, λ appearing in Eqs. (3) and (4) is assumed to be independent of D. It is simply given by $\lambda = \sqrt{A/K}$, which provides an upper bound for the width $W_{m,x}^{\mathrm{mic}}$ from the micromagnetic simulations. As shown in Fig. 3, the analytical value $W_{m,y}^{\mathrm{ana}}$ provides a good approximation for the width $W_{m,y}^{\mathrm{mic}}$ determined from micromagnetic calculations. However, these two quantities do not capture the unique shape of DW skyrmions. We therefore propose an alternative way to define the skyrmion size and shape using the topological charge density [34],

$$\varrho_{\mathrm{top}} = \frac{1}{4\pi}\boldsymbol{m}\cdot(\partial_x\boldsymbol{m}\times\partial_y\boldsymbol{m}). \tag{12}$$

The size of an arbitrary skyrmion can now be defined as the area enclosing a certain percentage of the topological charge. Normalized plots of topological charge density are shown in Fig. 2. The core of the DW skyrmion defined by $W_{m,x}$ and $W_{m,y}$ contains about 20% of the topological charge of the DW skyrmion.

Figure 3(b) shows the DW skyrmion energy versus D in units of k_bT for $T = 300$ K for analytical and micromagnetic calculations, which have near perfect agreement in the low D regime. For larger D, the fixed λ approximation becomes less valid, causing the analytical solution to deviate from the micromagnetic one.

IV. LORENTZ TEM SIMULATIONS

To support future experimental imaging of DW skyrmions, we employ Fresnel-mode Lorentz TEM calculations on the micromagnetic output of Fig. 2. Fresnel-mode Lorentz TEM is an out-of-focus imaging technique in which a through-focus series of bright-field images is recorded; details regarding the simulation of relevant image contrast can be found in Ref. [35]. Numerical profiles of an isolated VBL ($D = 0$ mJ/m^2) and an isolated DW skyrmion ($D = 0.5$ mJ/m^2) are illustrated in Figs. 2(f) and 2(i), respectively, which are used in the calculations of Fig. 4. In the absence of DMI, Bloch walls are present which display a sharp magnetic contrast that reverses at the location of the VBL in Fresnel-mode images [Fig. 4(a)]. In the presence of DMI, Néel walls become the preferred configuration and do not display any magnetic contrast in Fresnel-mode images without sample tilt. However, strong magnetic contrast is still observed at the location of the DW skyrmion in Fig. 4(d). This dipolelike contrast originates from the Bloch-like portions of the DW across the DW skyrmion. Thus, DW skyrmions would be the only contributor to magnetic contrast in systems that exhibit DMI when examined with Lorentz TEM in the absence of sample tilt.

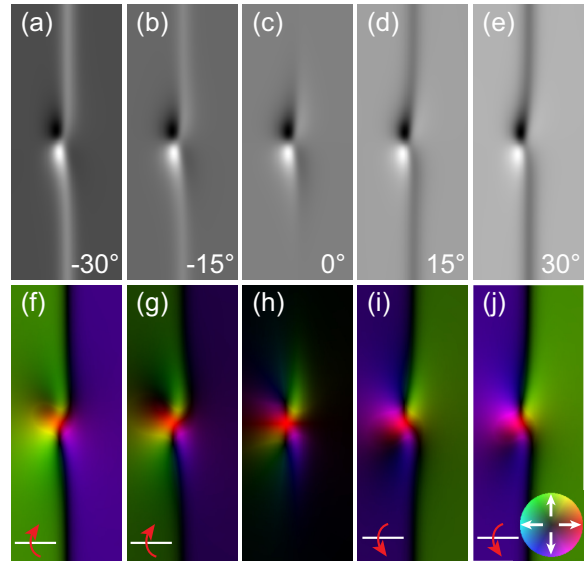

FIG. 5. (a)–(e) Fresnel-mode LTEM images and (f)–(j) corresponding in-plane magnetic induction maps of an isolated DW skyrmion ($D = 0.5$ mJ/m^2) at varied states of tilt calculated from micromagnetic outputs illustrated in Fig. 2(i).

As experimental Fresnel-mode Lorentz TEM images do not offer explicit directional information regarding the magnetic induction, phase reconstruction is typically employed using the transport of intensity equation (TIE) to calculate the integrated in-plane magnetic induction [36,37]. The resultant phase map for $D = 0$ displays contrast along the domain wall which reverses at the location of the VBL similar to that observed in the Fresnel-mode image. The color map shows the direction of in-plane induction matching those in the output of the micromagnetic simulation with a discontinuity at the location of the VBL. The magnetic induction takes on a distinct braidlike appearance centered around the DW skyrmion with no signal from the surrounding DW. This signature takes on a larger footprint than that of magnetic contrast in the calculated Fresnel-mode image which may assist in locating DW skyrmions in experimental images.

As mentioned previously, Néel walls do not display magnetic contrast in the absence of a sample tilt in Fresnel-mode imaging. When a tilt is applied to the sample, an in-plane component emerges from the perpendicular induction of neighboring domains giving rise to contrast at a Néel wall. This too is observed in our calculated Fresnel-mode images [Figs. 5(a)–5(e)]; as the sample tilt increases, the magnetic contrast becomes more apparent along the DW surrounding the DW skyrmion. Additionally, the contrast from the DW

skyrmion itself remains strong with respect to the surrounding DW regardless of the tilt direction, which will be useful for confirming the presence of a DW skyrmion experimentally. The corresponding in-plane magnetic induction maps [Figs. 5(f)–5(j)] further support this notion as the braidlike feature from the DW skyrmion remains visible even at larger tilts where a strong signal is observed around the DW.

V. SUMMARY

In summary, we have introduced a kind of topological magnetic excitation called a DW skyrmion characterized by a 360° transition of the internal magnetization within a Dzyaloshinskii DW and defined by a topological charge of ± 1. The DW skyrmion analysis presented here builds off prior work on VBLs in much the same way the recent surge in skyrmion research is rooted in decades of research on magnetic bubble memory. The static properties were calculated both analytically and micromagnetically with excellent agreement on the resulting size, energy, and profile. Although open questions remain about their thermal stability and dynamic properties, DW skyrmions provide an alternative strategy for leveraging topological protection in magnetic systems with a strong interfacial DMI. The reconfigurable nature of the DWs that host these excitations could open the door to different kinds of memory and computing schemes based on topological charge. To this end, we have proposed an experimental methodology to unequivocally image DW skyrmions using Fresnel-mode Lorentz TEM to support future work in this area.

ACKNOWLEDGMENTS

This work is financially supported by the Defense Advanced Research Project Agency (DARPA) program on Topological Excitations in Electronics (TEE) under Grant No. D18AP00011. C.M. and A.S. would also like to acknowledge support by NSF-CAREER Grant No. 1452670.

[1] I. Dzyaloshinsky, J. Phys. Chem. Solids **4**, 241 (1958).
[2] T. Moriya, Phys. Rev. **120**, 91 (1960).
[3] X. Z. Yu, Y. Onose, N. Kanazawa, J. H. Park, J. H. Han, Y. Matsui, N. Nagaosa, and Y. Tokura, Nature (London) **465**, 901 (2010).
[4] S. X. Huang and C. L. Chien, Phys. Rev. Lett. **108**, 267201 (2012).
[5] A. Thiaville, S. Rohart, E. Jué, V. Cros, and A. Fert, Europhys. Lett. **100**, 57002 (2012).
[6] A. Hrabec, N. A. Porter, A. Wells, M. J. Benitez, G. Burnell, S. McVitie, D. McGrouther, T. A. Moore, and C. H. Marrows, Phys. Rev. B **90**, 020402(R) (2014).
[7] J. P. Pellegren, D. Lau, and V. Sokalski, Phys. Rev. Lett. **119**, 027203 (2017).
[8] D. Lau, J. P. Pellegren, H. T. Nembach, J. M. Shaw, and V. Sokalski, Phys. Rev. B **98**, 184410 (2018).
[9] J. E. Hirsch, Phys. Rev. Lett. **83**, 1834 (1999).
[10] L. Q. Liu, C.-F. Pai, Y. Li, H. W. Tseng, D. C. Ralph, and R. A. Buhrman, Science **336**, 555 (2012).
[11] S. Emori, U. Bauer, S.-M. Ahn, E. Martinez, and G. S. D. Beach, Nat. Mater. **12**, 611 (2013).
[12] A. Hoffmann, IEEE Trans. Magn. **49**, 5172 (2013).
[13] W. J. Jiang, P. Upadhyaya, W. Zhang, G. Q. Yu, M. B. Jungfleisch, F. Y. Fradin, J. E. Pearson, Y. Tserkovnyak, K. L. Wang, O. Heinonen, S. G. E. te Velthuis, and A. Hoffmann, Science **349**, 283 (2015).
[14] S. Woo, K. Litzius, B. Krüger, M.-Y. Im, L. Caretta, K. Richter, M. Mann, A. Krone, R. M. Reeve, M. Weigand, P. Agrawal, I. Lemesh, M.-A. Mawass, P. Fischer, M. Kläui, and G. S. D. Beach, Nat. Mater. **15**, 501 (2016).
[15] P. Jennings and P. Sutcliffe, J. Phys. A: Math. Theor. **46**, 465401 (2013).
[16] S. B. Gudnason and M. Nitta, Phys. Rev. D **89**, 085022 (2014).
[17] A. Thiaville, J. Magn. Magn. Mater. **140-144**, 1877 (1995).
[18] A. P. Malozemoff and J. C. Slonczewski, Phys. Rev. Lett. **29**, 952 (1972).
[19] J. C. Slonczewski, J. Appl. Phys. **45**, 2705 (1974).
[20] S. Konishi, IEEE Trans. Magn. **19**, 1838 (1983).
[21] S. Konishi, K. Matsuyama, I. Chida, S. Kubota, H. Kawahara, and M. Ohbo, IEEE Trans. Magn. **20**, 1129 (1984).
[22] W. Jiang, X. Zhang, G. Yu, W. Zhang, X. Wang, M. Benjamin Jungfleisch, J. E. Pearson, X. Cheng, O. Heinonen, K. L. Wang, Y. Zhou, A. Hoffmann, and S. G. E. te Velthuis, Nat. Phys. **13**, 162 (2016).
[23] S. Mühlbauer, B. Binz, F. Jonietz, C. Pfleiderer, A. Rosch, A. Neubauer, R. Georgii, and P. Böni, Science **323**, 915 (2009).
[24] S. V. Tarasenko, A. Stankiewicz, V. V. Tarasenko, and J. Ferré, J. Magn. Magn. Mater. **189**, 19 (1998).
[25] A. Hubert and R. Schäfer, *Magnetic Domains: The Analysis of Magnetic Microstructures* (Springer, Berlin, 1998).
[26] A. V. Nikiforov and E. B. Sonin, JETP **63**, 766 (1986).
[27] O. Boulle, S. Rohart, L. D. Buda-Prejbeanu, E. Jué, I. M. Miron, S. Pizzini, J. Vogel, G. Gaudin, and A. Thiaville, Phys. Rev. Lett. **111**, 217203 (2013).
[28] Micromagnetic code M^3, http://magneticslab.ua.edu/micromagnetics-code.html.
[29] J. B. Mohammadi, K. Cole, T. Mewes, and C. K. A. Mewes, Phys. Rev. B **97**, 014434 (2018).
[30] S. Rohart and A. Thiaville, Phys. Rev. B **88**, 184422 (2013).
[31] M. J. Donahue and D. G. Porter, Physica B **343**, 177 (2004).
[32] X. S. Wang, H. Y. Yuan, and X. R. Wang, Commun. Phys. **1**, 31 (2018).
[33] See Supplemental Material at http://link.aps.org/supplemental/10.1103/PhysRevB.99.184412 for a definition of the DW skyrmion widths, which includes Refs. [25,38–40].
[34] S. Heinze, K. von Bergmann, M. Menzel, J. Brede, A. Kubetzka, R. Wiesendanger, G. Bihlmayer, and S. Blügel, Nat. Phys. **7**, 713 (2011).
[35] M. De Graef, in *Magnetic Microscopy and its Applications to Magnetic Materials*, edited by M. De Graef and Y. Zhu, Experimental Methods in the Physical Sciences, Vol. 36 (Academic, New York, 2000), Chap. 2.
[36] D. Paganin and K. A. Nugent, Phys. Rev. Lett. **80**, 2586 (1998).
[37] M. Beleggia and Y. Zhu, Philos. Mag. **83**, 1045 (2003).
[38] J. Barzilai and J. M. Borwein, IMA J. Numer. Anal. **8**, 141 (1988).
[39] A. Cauchy, C.R. Acad. Sci. Paris **25**, 536 (1847).
[40] Y.-H. Dai and Y.-X. Yuan, IMA J. Numer. Anal. **23**, 377 (2003).